

X-ray phase-contrast imaging

Marco Endrizzi^a

^a*Department of Medical Physics and Biomedical Engineering, University College London,
Gower Street, London WC1E 6BT, United Kingdom*

Abstract

X-ray imaging is a standard tool for the non-destructive inspection of the internal structure of samples. It finds application in a vast diversity of fields: medicine, biology, many engineering disciplines, palaeontology and earth sciences are just few examples. The fundamental principle underpinning the image formation have remained the same for over a century: the X-rays traversing the sample are subjected to different amount of absorption in different parts of the sample. By means of phase-sensitive techniques it is possible to generate contrast also in relation to the phase shifts imparted by the sample and to extend the capabilities of X-ray imaging to those details that lack enough absorption contrast to be visualised in conventional radiography. A general overview of X-ray phase contrast imaging techniques is presented in this review, along with more recent advances in this fast evolving field and some examples of applications.

Keywords: X-ray; phase-contrast; imaging

1. Introduction

2 The use of X-rays for imaging the internal structure of samples quickly spread
3 around the world soon after the first X-ray radiograph was taken by Wilhelm
4 Conrad Röntgen towards the end of 1895 [1]. Great improvements have con-
5 stantly been made throughout the last century both with regard to the X-ray
6 generators and to the image receptors, including transformative advances such

Email address: m.endrizzi@ucl.ac.uk (Marco Endrizzi)

7 as the introduction of tomography [2]. X-ray imaging is nowadays a standard
8 tool in many diverse fields and disciplines, ranging from medical sciences to ma-
9 terials engineering and including quality control in industry as well as security
10 screening.

11 Despite tremendous progress, the fundamental working principle has re-
12 mained unchanged for over a century: contrast is generated by differences in the
13 absorption of the X-rays within the sample. This can provide excellent results
14 when relatively high attenuation exists, but leads to poor image quality when the
15 sample is weakly absorbing. Generally speaking, this occurs for materials and
16 tissues composed of light elements. The possibility of performing phase-based
17 imaging bears the potential of making visible what would be undetectable with
18 the conventional method for these classes of samples.

19 A number of reviews is already available on this topic, including a focus
20 on the evolution and relative merits of these imaging techniques [3], on the
21 transition from synchrotron to conventional sources [4], on medical applications
22 [5–7] with the translation towards clinical implementation [8] the imaging of the
23 breast [9], and also on materials science applications [10, 11].

24 The aim of this review is to present a general overview of the essentials X-
25 ray phase-contrast imaging techniques in the hard X-ray regime, as well as some
26 examples of use in applied investigations. An in-depth discussion is dedicated
27 to the principles and recent advances of edge illumination, a technique that has
28 been intensively investigated in the recent time by our group for the translation
29 of these advanced X-ray imaging techniques into table-top instrumentation that
30 can be compatible with clinical or industrial environments.

31 **2. Methods**

32 X-ray imaging is a general term that embraces an extremely wide set of tech-
33 niques that are used to produce a representation of the sample under inspection.
34 In order to describe phase-contrast X-ray imaging techniques, we will start from
35 the basis of the more conventional, or absorption-based, approach.

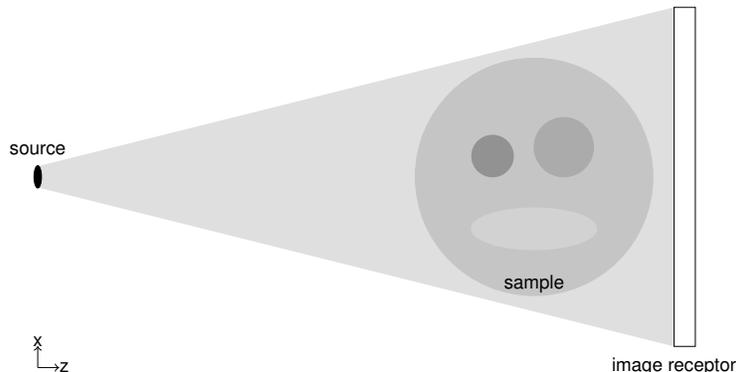


Figure 1: Schematic of the set-up for conventional X-ray imaging: the image receptor looks directly at the radiation source and through the sample.

36 *2.1. Absorption imaging*

37 The sketch in Figure 1 reports the arrangement that is typically used in ra-
 38 diography by using an X-ray source and an image receptor. It is a transmission-
 39 type imaging modality in which the image receptor looks at the source and
 40 through the sample. The internal structure of the sample can be inspected in
 41 this way because the differences in the attenuation of the X-rays, along their
 42 trajectories from the generator to the receptor, produce contrast. In order to
 43 quantify this effect we will use a two dimensional representation of a simple
 44 object, a sphere made of a single material embedded into another homoge-
 45 neous material. This situation is depicted in Figure 2 where panel 2a shows
 46 the arrangements of X-ray radiation, phantom and detector while the panel 2b
 47 the resulting image. The coordinate system is defined as follows: the X-rays
 48 propagate from the source along the z axis, the object extends in all the three
 49 dimensions and the image at the receptor is a two dimensional distribution of
 50 intensity in the (x, y) plane. By using monochromatic radiation of wavelength
 51 λ , the intensity at the detector can be described by using the Beer-Lambert law
 52 [13]

$$I(x, y) = I_0(x, y) \exp [-(\mu_o^\lambda - \mu_h^\lambda)T_o(x, y)] \quad (1)$$

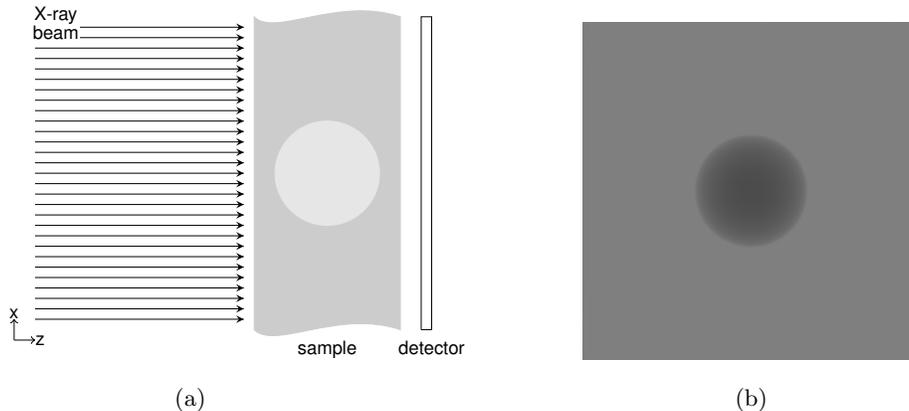


Figure 2: (a) simple model for the generation of contrast in absorption-based X-ray imaging. (b) corresponding image recorded represented as the two dimensional distribution of intensity, which was computed by using the X-Tract software [12].

53 where $T_o(x, y)$ is the projected thickness of the object on the (x, y) plane and
 54 $I_0(x, y)$ is the intensity incident on the sample. For the simple case presented
 55 above this can be calculated analytically. Let us assume a sphere of radius r
 56 and centred in the origin. The projected thickness of the sphere, measured by a
 57 line profile running across the centre of the sphere ($y = 0$), is given by the real
 58 part of

$$T(x) = 2\sqrt{r^2 - x^2}. \quad (2)$$

59 We can then calculate the corresponding intensity profile by using Equation 1.
 60 In order to do so we need to specify the working energy (30 keV), the materials
 61 (aluminium for the sphere and water for the embedding material) and we further
 62 assume a constant incident intensity $I_0(x, y) = 1$.

63 It is often the case, for example when using conventional laboratory sources
 64 such as X-ray tubes, that the radiation is polychromatic and its spectrum ex-
 65 tends over a range of several tens of keV. This can be included in Equation 1 by
 66 an integration over the energy that takes into account the energy dependence of
 67 the source spectrum $I_0(\lambda)$, of the attenuation coefficient μ^λ and of the detector

68 response $\mathcal{D}(\lambda)$

$$I(x, y) = \int d\lambda I_0(x, y; \lambda) \exp [-(\mu_o^\lambda - \mu_h^\lambda)T_o(x, y)] \mathcal{D}(\lambda). \quad (3)$$

69 Each monochromatic component of the X-ray beam contributes independently
70 to the contrast, with a weight that is equal to the relative probability of emis-
71 sion and detection, and with the attenuation coefficient characteristic of that
72 particular energy (for example see [14]).

73 2.2. Phase-contrast imaging

74 The phase of the waves travelling through the sample contributes to the
75 modulation of the detected intensity in an X-ray phase-contrast imaging system.
76 This can be described by means of the complex refractive index [15]

$$n = 1 - \delta + i\beta \quad (4)$$

77 where the decrement to unity δ governs the phase shifts while β the absorption.
78 Away from absorption edges, and in the region where the photoelectric effect
79 dominates absorption, δ and β can be expressed as functions of the electron
80 density ρ and of the radiation wavelength in the following way [16]

$$\delta(\lambda) = \rho \frac{r_e \lambda^2}{2\pi} \quad (5)$$

$$\beta(\lambda) = \mu(\lambda) \frac{\lambda}{4\pi} \quad (6)$$

81 where r_e is the classical electron radius. It is worth noting that δ is typically
82 larger than β . By taking for example water at 30 keV, we obtain $\delta \approx 2.56 \cdot 10^{-7}$
83 and $\beta \approx 1.36 \cdot 10^{-10}$. Another key difference between the two parameters is their
84 dependence on the X-ray energy E : β decreases approximately with E^{-4} while
85 δ approximately as E^{-2} . Real and imaginary parts of the complex refractive
86 indices of two materials, one composed of light elements and one composed of
87 heavier elements, are plotted in Figure 3 in the energy range between 10 and
88 120 keV for illustration purposes.

89 The phase shift imparted by the sample to the X-ray wave is given by

$$\Phi(x, y; \lambda) = -k \int_{\mathcal{O}} dz \delta(x, y, z; \lambda) \quad (7)$$

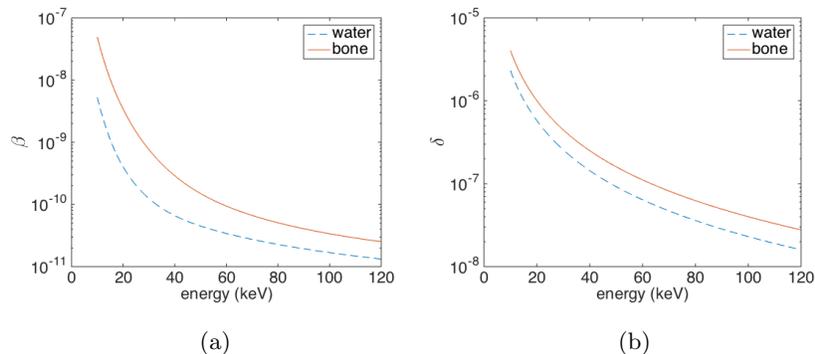


Figure 3: Complex index of refraction for water and bone as a function of X-ray energy: (a) β and (b) δ . Bone composition was taken from the ICRU report [17].

90 where the integration is carried out over the extent of the object \mathcal{O} along the
 91 optical axis, and this Equation can be considered valid for propagation through
 92 thin objects, for which the projection approximation holds [15].

93 Referring to previous example of a simple sphere composed of a single ma-
 94 terial, the transmission and phase shift of the sample become

$$I(x, y; \lambda) = \exp \left[-\frac{4\pi\beta(\lambda)}{\lambda} T(x, y) \right] \quad (8)$$

$$\phi(x, y; \lambda) = -k \delta T(x, y) \quad (9)$$

95 where a single energy was used for the X-ray beam.

96 3. X-ray phase-contrast imaging

97 It is not possible to directly measure the phase of electromagnetic waves
 98 at optical frequencies and above, however, phase effects can play a significant
 99 role in the image formation also in the hard X-ray regime. Phase-contrast
 100 imaging techniques exploit the phase perturbations introduced by the sample
 101 to modulate the intensity recorded at the image receptor, in such a way that
 102 these effects can be detected and interpreted.

103 A summary of these techniques will be presented in the following sections.
 104 The classification is inevitably made afterwards, and it is therefore natural that

105 the categories will be appropriate in certain cases while less accurate in others.
 106 X-ray phase-contrast imaging techniques are evolving fast, and a large degree
 107 of contamination often exists across different approaches. A classification based
 108 on the most prominent characteristics of the experimental set-ups and their
 109 working principles was chosen here as the main criterion for distinction between
 110 different approaches.

111 3.1. Interferometry

112 The first example of X-ray phase-contrast imaging method is the X-ray in-
 113 terferometer [18, 19] which was built from a monolithic crystal and used a Laue-
 114 Laue configuration. A schematic representation of this device is shown in
 Figure 4. Phase-coherent beams are formed by dividing the incoming X-ray

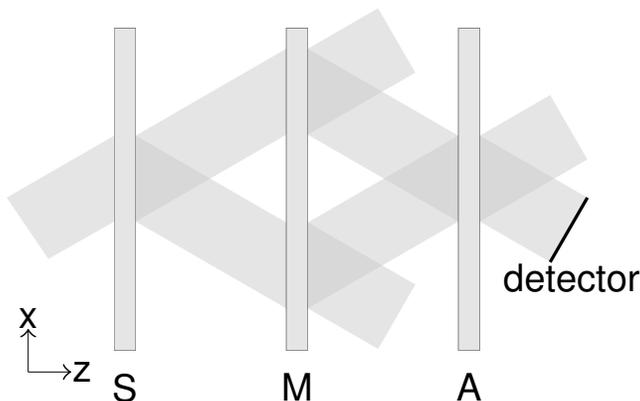


Figure 4: Top view of an X-ray interferometer.

115
 116 beam at the beam splitter S and successively at the transmission element M,
 117 they meet again at the analyser A where an atomic-scale standing wavefield is
 118 formed [20]. In an ideal scenario, where the wave is perfectly planar and the
 119 crystal free of imperfections, the field would be perfectly uniform until a sample
 120 is introduced in one of the arms of the interferometer. The image would then
 121 record the phase changes induced by sample, modulo 2π . In practice, local phase
 122 shifts, arising for example from strain and defects in the crystal, will generate
 123 interference patterns that will be superimposed to the modulations imposed by

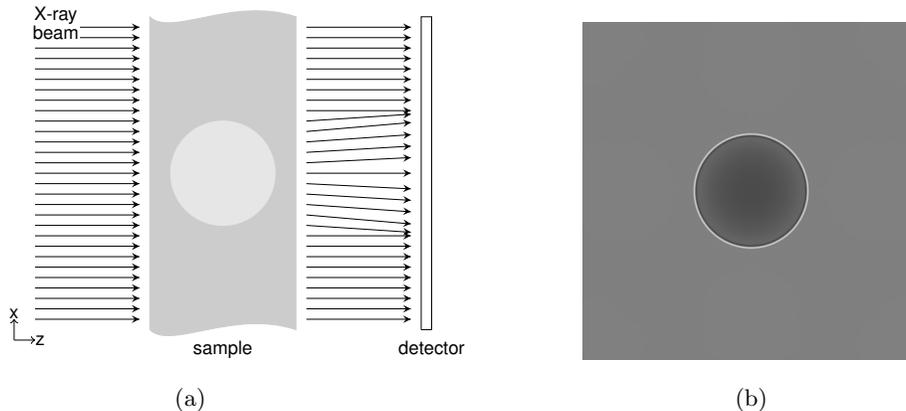


Figure 5: (a) simple model for the generation of a phase contrast image with the free space propagation technique. (b) corresponding image recorded represented as the two dimensional distribution of intensity, calculated by using the X-Tract software [12].

124 the sample. It is also possible to insert a known phase modulation in one arm,
 125 as for example a linear phase ramp imposed by using a wedge, while the sample
 126 under study is placed in the other arm. The linear phase ramp will generate a
 127 series of linear fringes in the intensity recorded at the detector, hence the name
 128 of fringe scanning method [21].

129 Following the first demonstration of the working principle and pioneering
 130 imaging experiments [22, 23], this method was used for biomedical imaging
 131 experiments [24–27] to study different tissue types such as breast, brain and
 132 blood [28–30].

133 3.2. Free-space propagation

134 Free-space propagation techniques are perhaps the ones requiring the sim-
 135 plest set-up because the introduction of an appropriate propagation distance R_2
 136 between the sample and the image receptor can be sufficient to make phase ef-
 137 fects detectable (see Figure 5). Early works demonstrating this possibility date
 138 back to the mid '90s and used both monochromatic and collimated synchrotron
 139 radiation [31, 32] and polychromatic radiation from a microfocus X-ray tube
 140 [33]. This phenomenon can be interpreted in terms of Fresnel diffraction and

141 key features of this approach to imaging can be identified by referring to the
 142 following expression [15, 33, 34]

$$I(x, y; M, \lambda) = \frac{I_0}{M^2} \left[1 + \frac{R_2 \lambda}{M 2\pi} \nabla_{\perp}^2 \phi(x, y; R_1, \lambda) \right] \quad (10)$$

143 that describes the intensity distribution at the image receptor plane from a pure
 144 phase object. $M = (R_1 + R_2)/R_1$ is the geometrical magnification. The contrast
 145 from a pure phase object vanishes when $R_2 \rightarrow 0$, which is the typical condition
 146 for conventional (contact) radiography and the phase term is directly propor-
 147 tional to the propagation distance R_2 . Another feature of interest is that the
 148 monochromaticity of the radiation is not essential for this type of imaging. A
 149 necessary condition, however, is that the radiation must have a certain degree
 150 of spatial coherence [13]:

$$l_c = \frac{\lambda R_1}{\sigma_s 2\sqrt{2 \log 2}} \quad (11)$$

151 where σ_s is the standard deviation of the source intensity distribution. The
 152 coherence length l_c has to be comparable to or larger than the inverse spatial
 153 frequency of the feature of interest [35] in order to obtain significant phase con-
 154 trast. In practice this means that the source has to be relatively small or that
 155 the object must be placed at a relatively large distance R_1 from it. Another re-
 156 quirement is that the imaging system must have spatial resolution high enough
 157 to not wash out the interference fringes. This is conveniently summarised by
 158 the following expression [36, 37]

$$\sigma_t^2 \approx \left(1 - \frac{1}{M} \right)^2 \sigma_s^2 + \frac{\sigma_d^2}{M^2} + \sigma_m^2 \quad (12)$$

159 where σ_t and σ_d are the standard deviations of the system's and of the detec-
 160 tor's point spread function, respectively. Another point to be noted is that the
 161 diffraction term

$$\sigma_m = \frac{1}{2} \sqrt{\frac{\lambda R_2}{2}} \quad (13)$$

162 becomes less significant for increasing X-ray energies.

163 The intensity projection image, acquired with a certain propagation distance
 164 between the sample and the detector, will contain a mixture of contributions

165 from both the absorption and the phase shifts in the sample. Other experimental
166 parameters, like the X-ray energy, the geometrical magnification, the radiation
167 coherence and the system resolution, determine the modulation of intensity at
168 the detector. The process that aims at making this type of imaging quantitative
169 by calculating phase and amplitude at the exit surface of the sample is called
170 phase retrieval. Methods to achieve this, in the case of non-interferometric hard
171 X-ray imaging techniques, started developing soon after the first experiments
172 [38–41], also including polychromatic X-ray beams [42] and even exploiting dif-
173 ferent energies for the phase retrieval process itself [43]. Quantitative retrieval
174 algorithms are also a fundamental component for accurate three-dimensional
175 reconstructions [44–46]. In general terms, the determination of both amplitude
176 and phase requires more than a single measurement (for example by changing
177 the propagation distance or by changing the energy) unless some constraints can
178 be imposed on the sample. Quantitative phase retrieval can be performed from
179 a single defocus distance by requiring homogeneity of the sample [47]: although
180 this might not always be strictly satisfied, it is a very reasonable approxima-
181 tion in many cases of interest (e.g. soft tissue samples) and this approach often
182 delivers high quality projections and reconstructions.

183 Applications of free-space propagation X-ray phase-contrast imaging are vast
184 and definitely too many to be covered here. We will limit this discussion to few
185 highlights like micro- and nano-tomography applications [48–54], lung imaging
186 [55–59] and breast tissue imaging [60, 61] including in-vivo [62–64].

187 *3.3. Analyser based imaging*

188 Analyser-based methods make use of crystals both for beam preparation and
189 analysis. The crystal arrangement preceding the sample is used to monochro-
190 matise and collimate the incoming X-ray beam while the one preceding the
191 detector serves as a fine angular filter. A typical synchrotron experimental set-
192 up is sketched in Figure 6. The X-ray beam is usually wide enough to cover
193 the extent of the sample along the x direction while scanning along y is often
194 necessary to build a two-dimensional image. The intensity at the detector is

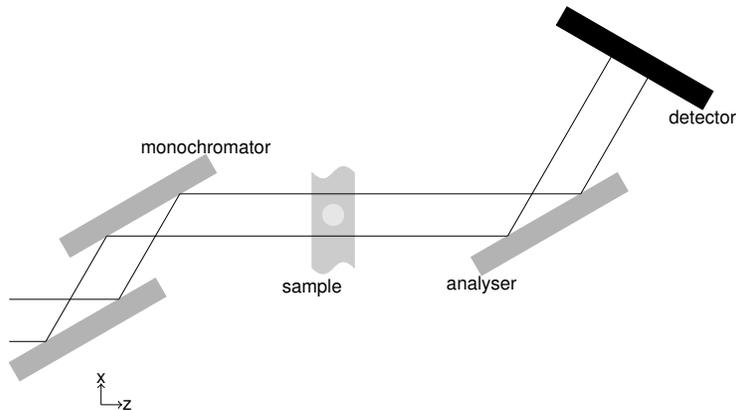


Figure 6: Example of analyser based imaging set-up.

195 modulated by changing the angle of incidence of the X-ray beam on the second
 196 (analyser) crystal (see Figure 7a). This characteristic curve takes the name of
 197 rocking curve and it is key in the image formation process. It results from the
 198 combination of the reflectivity curves of both the monochromator and the anal-
 199 yser crystal with a contribution arising from the beam divergence [65]. When
 200 the system is tuned in such a way that roughly half of the intensity reaches the
 201 detector (at full width half maximum of the rocking curve), small changes in
 202 the direction of the propagation of the X-rays due to refraction in the sample
 203 are transformed into intensity changes at the image receptor. The change in
 204 direction of propagation is directly proportional to the gradient of the sample's
 205 phase [13]

$$\theta_R = \frac{\lambda}{2\pi} \frac{\partial \phi(x, y)}{\partial x} \quad (14)$$

206 and an imaging system where contrast is proportional to the refraction angle
 207 is often referred to as differential phase-contrast imaging system. The image
 208 recorded in the case of the sphere sample is shown in Figure 7b. The X-rays
 209 going through the centre of the sphere experience little or no refraction at all,
 210 therefore their direction of propagation is not changed and they are transmitted
 211 by the analyser with the same probability of the radiation that is not hitting
 212 the sample. The image contrast in this region of the sample is mainly due to

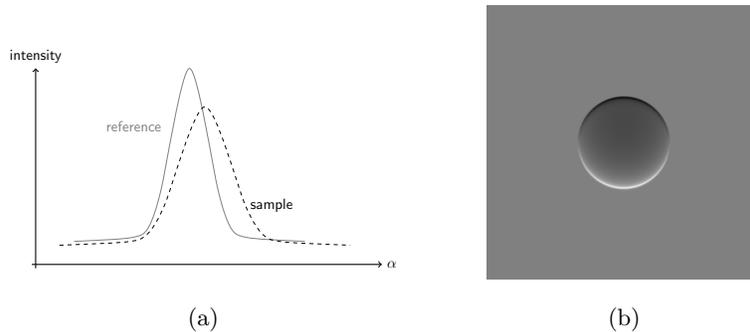


Figure 7: Image formation principle in an analyser-based system. (a) typical rocking curve: intensity recorder at a fixed position in the detector plane as a function of the “rocking” angle α of the analyser crystal. (b) intensity recorded at the detector when the analyser crystal is set at fixed angle, in such a way that 50% of the intensity is transmitted (obtained by using the X-Tract software [12]).

213 X-ray absorption within the sample. Refraction increases while approaching the
 214 sphere’s edges, where the change in the direction of propagation is maximum.
 215 Because X-rays are deflected away from the beam axis (a glass sphere in air acts
 216 as a diverging lens in the X-ray regime), the angle of incidence of the radiation on
 217 the analyser will be changed in two opposite ways at the two edges of the sphere.
 218 On one side, this will result in a higher probability of transmission through the
 219 analyser, while it will translate into a smaller transmission probability on the
 220 opposite side. This is the mechanisms at the basis of the generation of the dark
 221 and bright fringes of Figure 7b.

222 Early implementations of this technique for imaging fusion pellets are those
 223 of Goetz and Forster [66, 67]. This approach became increasingly popular after
 224 1995 [68, 69] when methods to quantitatively separate phase and absorption
 225 contributions were developed [70, 71]. This method is intrinsically sensitive to
 226 the phase gradient in a single direction only and an additional measurement
 227 is tipycally required to quantify the other component [72]. Another key de-
 228 velopment that soon followed was the possibility to quantify the effect of the
 229 scattering in the sample on the width of the rocking curve, which was put in
 230 relation to sub-pixel scale features [73–77]. This was also extended for applica-

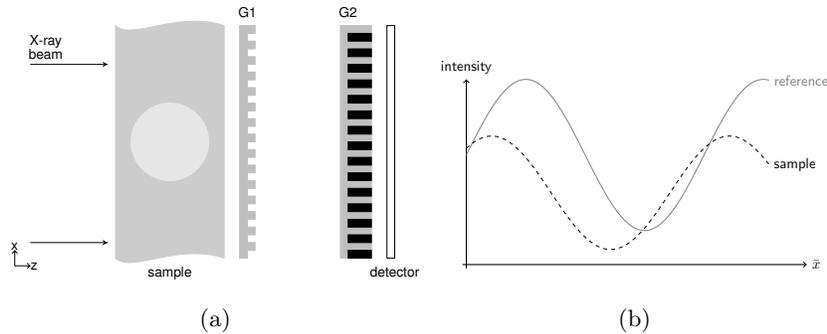


Figure 8: Example of grating based imaging set-up. (a) typical arrangement where the phase grating is placed after the sample and the (analyser) amplitude grating immediately precedes the detector. (b) intensity recorded at a fixed (x, y) position in the detector plane as a function of the scanning position of one grating relative to the other, along the x direction.

231 tions to tomography [78]. Methods for retrieving phase information from the
 232 simultaneous acquisition of two images have been developed for the case of Laue
 233 analyser [79].

234 Some examples of the many applications of analyser based techniques in
 235 the medical field [80] are: cartilage [81–83], musculoskeletal [84] and breast
 236 tissue [65, 85–87] imaging and dynamic tracking of micro-bubble concentrations
 237 [88, 89].

238 3.4. Grating based imaging

239 Grating-based imaging methods make use of periodic structures to condition
 240 and analyse the X-ray beam. A typical embodiment of this technique is sketched
 241 in Figure 8a where the X-ray beam traverses the sample that modulates its
 242 amplitude and imposes phase shifts. It is then passed through the phase grating
 243 G_1 and analysed by the absorption grating G_2 immediately before the image
 244 receptor. If one of the two grating is laterally scanned (along x) without the
 245 sample in the beam, a modulated intensity curve is detected in each pixel. This is
 246 often referred to as the phase-stepping curve. When the sample is present in the
 247 beam, this curve is modified in three ways, as depicted in Figure 8b. The relative
 248 reduction of the baseline is the conventional absorption image, the lateral shift of

249 the curve represents the differential phase contrast and the reduction of visibility
 250 is linked to the scattering in the sample, or dark-field imaging. This can be
 251 expressed quantitatively by writing the intensity oscillations recorded at a point
 252 (x, y)

$$I(\bar{x}; x, y) = \sum_i a_i(x, y) \cos\left(\frac{2\pi i \bar{x}}{p_2} + \Phi_i(x, y)\right) \quad (15)$$

$$\approx a_0(x, y) + a_1(x, y) \cos\left(\frac{2\pi i \bar{x}}{p_2} + \Phi_1(x, y)\right) \quad (16)$$

253 where p_2 is the period of G_2 and a_i and Φ_i are the amplitude and phase coefficient,
 254 respectively. The images of the sample are reconstructed by comparing
 255 the phase-stepping curves recorded without w and with o the sample in the
 256 beam [90]. The transmission image, analogous to the one obtained in conventional
 257 radiography, is given by

$$T(x, y) = a_0^o(x, y)/a_0^w(x, y). \quad (17)$$

258 The differential phase-contrast projection image of the sample is calculated by
 259 taking the difference $\nabla_x \phi(x, y) = \nabla_x^o \phi(x, y) - \nabla_x^w \phi(x, y)$, and by considering
 260 that

$$\nabla_x \phi(x, y) = \frac{p_2}{\lambda d} \Phi_1(x, y) \quad (18)$$

261 where d is the distance between G_1 and G_2 . Dark-field images are obtained by
 262 first computing the normalized oscillation amplitude

$$V^w(x, y) = \frac{I_{max}^w(x, y) - I_{min}^w(x, y)}{I_{max}^w(x, y) + I_{min}^w(x, y)} \quad (19)$$

$$= \frac{a_1^w(x, y)}{a_0^w(x, y)} \quad (20)$$

263 and then by taking the ratio of this quantity, with and without sample in the
 264 beam

$$V(x, y) = \frac{V^o(x, y)}{V^w(x, y)} \quad (21)$$

$$= \frac{a_1^o(x, y)a_0^w(x, y)}{a_1^w(x, y)a_0^o(x, y)} \quad (22)$$

265 which does not show changes ($V(x, y) = 1$) for samples with negligible or absent
266 small-angle scattering and is reduced ($V(x, y) < 1$) when scattering occurs.

267 Introduction of grating-based techniques could be dated back to early '90s
268 [91, 92] with experiments following few years later [93–97]. A breakthrough
269 for the diffusion of this technique was the introduction of a third grating that
270 enabled the use of low brilliance sources [98], tomography [99] and dark-field
271 [100] or scattering imaging were also developed soon afterwards with a three-
272 grating setup. An alternative method was subsequently proposed for differential
273 phase-contrast imaging with weakly coherent hard X-rays [101]. Quantitative
274 three-dimensional dark-field imaging was then developed for these grating-based
275 imaging set-ups [102, 103]. The simultaneous determination of the two compo-
276 nents of the phase gradient, by means of gratings structured in two dimen-
277 sions, has also been discussed [104–107]. Another important development is
278 the inverse geometry [108] which can enable compact Talbot-Lau interferome-
279 try setups [109]. A much more detailed review of advances and milestones of
280 grating-based X-ray phase-contrast imaging can be found in a recent review [90].
281 A recent and very promising development on this front was the successful fab-
282 rication of grating structures with approximately one order of magnitude finer
283 pitch [110] and their application for the enhancement of table-top imaging sys-
284 tems [111]. Albeit based on gratings, the working principle of this approach is
285 different from that of the more conventional grating-based interferometry and
286 it is best understood under the concept of univesal moiré effect [112]. This
287 eliminates the need for an absorption grating and enables the realization of
288 a polychromatic far-field interferometer that can overcome the limitations in
289 sensitivity and dose efficiency of more conventional bench-top interferometers
290 [112].

291 An extremely wide spectrum of application exists also for grating based
292 imaging techniques, examples are: breast tissue [113–115], brain tumour [116],
293 cartilage [117–120], and lungs [121, 122]. A fairly recent review exists that is
294 fully dedicated to this topic [123].

295 *3.5. Tracking based methods*

296 Another broad category of X-ray phase-contrast imaging techniques stems
297 from the observation that it is possible to measure the sample absorption, re-
298 fraction and scattering by imposing a known structure to the radiation field and
299 by directly tracking its modifications. In general terms, an overall reduction of
300 the structured beam intensity can be traced back to absorption of the radiation
301 within the sample, while the spatial distortions of the known intensity patterns
302 are used to infer the phase shifts imposed by the sample to the wavefront.

303 The introduction of this approach may be traced back to the ‘90s [124, 125]
304 with experiments following several years later. The structuring could be imposed
305 by using a lenslet array [126], a microprobe [127], an absorption grid [128–
306 130], a phase grating [131] or a speckle pattern [132, 133] and the distortions
307 imposed by the sample can be tracked by using a high-resolution detector, also
308 in combination with sub-pixel resolution analysis [134] or by using Fourier-based
309 analysis [135]. These approaches can be extended to two-dimensional sensitivity
310 [136–138], to include dark-field contrast [139, 140] and directional dark-field
311 imaging [141–143]; as well as three-dimensional imaging with tomography [142,
312 144].

313 Applications of tracking based techniques include: bone imaging [145], dy-
314 namic airways imaging [146, 147] and metrology [142, 148, 149].

315 **4. Edge illumination**

316 Edge illumination X-ray phase-contrast imaging has been investigated in
317 the recent years as a possible way forward for the translation of phase-sensitive
318 imaging techniques into mainstream applications. Edge illumination was ini-
319 tially developed in synchrotron experiments at Elettra (Italy) and was inspired
320 by analyser-based methods [150]. The typical experimental set-up is reported in
321 Figure 9a. A beam of synchrotron radiation, propagating from left to right, is
322 shaped down to a narrow blade of radiation by an aperture. It then traverses the
323 sample and impinges on the edge of a second aperture that is placed in front of

324 the image receptor. If one of the two apertures is laterally shifted (along x) the
 325 recorded intensity is modulated: it reaches a maximum when the two apertures
 326 are perfectly aligned and it progressively decreases for increasing lateral shifts
 327 (see Figure 9b). This is often called illumination function and characterises the
 properties of this type of imaging systems.

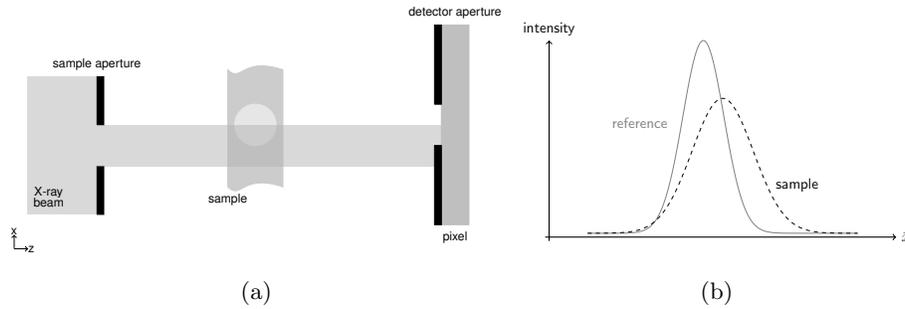


Figure 9: Edge illumination working principle: (a) typical synchrotron set-up and (b) illumination function.

328
 329 The working principle of edge illumination can be explained by observing
 330 that refraction in the sample results in lateral shifts of the X-ray beam which
 331 are translated into intensity modulations by the presence of the second aper-
 332 ture. Referring to Figure 9a, a deflection upwards will result in an increased
 333 intensity at the detector pixel while a decreased intensity would be recorded if
 334 the deflection occurs downwards. This holds for a completely transparent object
 335 that only perturbs the phase of the X-ray beam. If the sample is also absorbing,
 336 then at least two images have to be acquired to extract the sample's absorption
 337 and refraction [151]. This is typically achieved by recording two intensity pro-
 338 jections, with the apertures aligned in such a way that the shaped X-ray beam
 339 impinges on the two edges of the detector aperture. If the apertures are aligned
 340 such that half of the intensity reaches the detector in both cases, these two
 341 configurations correspond to the two points at the full width half maximum of
 342 the illumination function (see Figure 9b). The edge illumination principle can
 343 also be implemented with a laboratory set-up that uses rotating anode X-ray
 344 tubes with extended focal spots [152] (sketched in Figure 10). The diverging and

345 polychromatic beam generated by this type of sources is shaped by a pre-sample
 346 mask that creates a series of independent beamlets. These propagate through

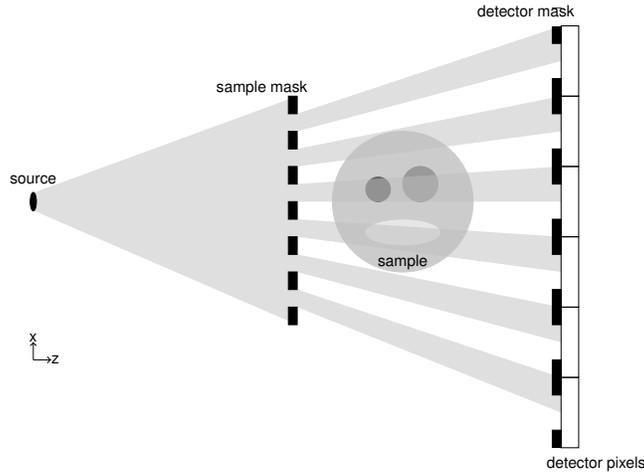


Figure 10: Laboratory set-up for edge illumination X-ray phase-contrast imaging.

346

347 the sample and are then analysed by a second set of apertures before the de-
 348 tector. The pitches of both the pre-sample and the detector mask are harmoni-
 349 cally matched to that of the detector pixels such that a one-to-one relationships
 350 exists between each aperture in both masks and each detector pixel column
 351 (along y). This approach has negligible spatial or temporal coherence require-
 352 ments [153, 154], provides high sensitivity also for laboratory implementations
 353 [155, 156], enables the simultaneous attainment of high sensitivity and dynamic
 354 range [157], is robust against thermal and mechanical instabilities [158, 159] and
 355 the set-up can be made compact [160, 161]. By using a microfocal source it is
 356 possible to adopt a large magnification geometry and perform hard X-ray phase
 357 imaging with micrometre resolution [162]. Two-dimensional sensitivity can be
 358 simultaneously achieved by using masks structured in two dimensions [163].

359 Dark-field images can be quantitatively retrieved by acquiring (at least) a
 360 third intensity projection [164, 165] and by using a Gaussian representation
 361 of the intensity. Under general conditions, the illumination function $L(\vec{x})$ (see

362 Figure 9b) can be expressed in the following way

$$I(\bar{x}) = \sum_m \sum_n A_{mn} \exp \left[-\frac{(\bar{x} - \mu_{mn})^2}{2\sigma_{mn}^2} \right] \quad (23)$$

363 where $\mu_{mn} = \mu_m + \mu_n$, $\sigma_{mn}^2 = \sigma_m^2 + \sigma_n^2$ and $A_{mn} = A_m A_n (1/\sqrt{2\pi\sigma_{mn}^2})$. Both
 364 the illumination function $L(\bar{x}) = \sum_n (A_n/\sqrt{2\pi\sigma_n^2}) \exp[-(\bar{x} - \mu_n)^2/2\sigma_n^2]$ and
 365 the object function $O(\bar{x}) = \sum_m (A_m/\sqrt{2\pi\sigma_m^2}) \exp[-(\bar{x} - \mu_m)^2/2\sigma_m^2]$ have been
 366 represented as the sum of Gaussian functions, ($m = 1 \dots M$ and $n = 1 \dots N$).
 367 A single-Gaussian representation of both illumination and object function is
 368 accurate in many practical cases and this allows for an analytic solution of
 369 Equation 23 [164]. Should this not be the case, the number of terms to be
 370 retained in Equation 23 can be increased and the sample's parameters retrieved
 371 numerically [159, 166].

372 Tomographic edge-illumination X-ray phase-contrast imaging was developed
 373 at synchrotron sources [167] and adapted to rotating anode tubes [168, 169],
 374 including three-dimensional dark-field imaging [157]. A reverse-projection re-
 375 construction method enabled a step change in the data acquisition strategy
 376 by allowing continuous rotation of the sample [170, 171]. More recent develop-
 377 ments include algorithms for robust reconstructions [172, 173] and a single-image
 378 phase retrieval algorithm [174] that, albeit requiring homogeneity of the sam-
 379 ple, greatly simplifies the practical implementation of the method especially with
 380 respect to tomography [175]. This can be extended to include multi-material
 381 samples [176].

382 Examples of use in applied investigations of edge illumination X-ray phase
 383 contrast imaging are: low-dose mammography [177, 178], cartilage imaging [179,
 384 180], security [181], baggage screening [182] with a large field of view scanning
 385 system [183–185], composites materials [186, 187], regenerative medicine [188]
 386 and lung imaging [189].

387 **5. Conclusion**

388 X-ray phase-contrast imaging can extend the applicability of radiography
389 and tomography for visualising the internal structure of samples that do not
390 exhibit enough absorption contrast. Various methods have been developed to
391 obtain phase contrast images in the hard X-ray regime, and they were intro-
392 duced and described along with examples of applications. The edge illumination
393 approach, that has been subject of investigation and developments by our group
394 in the recent years, was finally presented and discussed.

395 **6. Acknowledgements**

396 ME was supported by the Royal Academy of Engineering under the RAEng
397 Research Fellowships scheme. Fruitful discussion with the members of the Ad-
398 vanced X-ray Imaging Group at UCL is kindly acknowledged.

- 399 [1] W. Röntgen, Über eine neue Art von Strahlen: vorläufige Mitteilung,
400 Sitzungsber. Phys. Med. Gesell. (1895).
- 401 [2] G. N. Hounsfield, Computerized transverse axial scanning (tomography):
402 Part 1. description of system, The British Journal of Radiology 46 (552)
403 (1973) 1016–1022.
- 404 [3] S. Wilkins, Y. I. Nesterets, T. Gureyev, S. Mayo, A. Pogany, A. Stevenson,
405 On the evolution and relative merits of hard x-ray phase-contrast imag-
406 ing methods, Philosophical Transactions of the Royal Society of London
407 A: Mathematical, Physical and Engineering Sciences 372 (2010) (2014)
408 20130021.
- 409 [4] A. Olivo, E. Castelli, X-ray phase contrast imaging: From synchrotrons to
410 conventional sources, Rivista Del Nuovo Cimento 37 (9) (2014) 467–508.
- 411 [5] P. Suortti, W. Thomlinson, Medical applications of synchrotron radiation,
412 Physics in medicine and biology 48 (13) (2003) R1.

- 413 [6] R. Lewis, Medical phase contrast x-ray imaging: current status and future
414 prospects, *Physics in medicine and biology* 49 (16) (2004) 3573.
- 415 [7] S.-A. Zhou, A. Brahme, Development of phase-contrast x-ray imaging
416 techniques and potential medical applications, *Physica Medica* 24 (3)
417 (2008) 129–148.
- 418 [8] A. Bravin, P. Coan, P. Suortti, X-ray phase-contrast imaging: from pre-
419 clinical applications towards clinics, *Physics in medicine and biology* 58 (1)
420 (2012) R1.
- 421 [9] P. Coan, A. Bravin, G. Tromba, Phase-contrast x-ray imaging of the
422 breast: recent developments towards clinics, *Journal of Physics D: Ap-
423 plied Physics* 46 (49) (2013) 494007.
- 424 [10] A. Stevenson, T. Gureyev, D. Paganin, S. Wilkins, T. Weitkamp, A. Sni-
425 girev, C. Rau, I. Snigireva, H. Youn, I. Dolbnya, et al., Phase-contrast
426 x-ray imaging with synchrotron radiation for materials science applica-
427 tions, *Nuclear Instruments and Methods in Physics Research Section B:
428 Beam Interactions with Materials and Atoms* 199 (2003) 427–435.
- 429 [11] S. C. Mayo, A. W. Stevenson, S. W. Wilkins, In-line phase-contrast x-
430 ray imaging and tomography for materials science, *Materials* 5 (5) (2012)
431 937–965.
- 432 [12] T. E. Gureyev, Y. Nesterets, D. Ternovski, D. Thompson, S. W. Wilkins,
433 A. W. Stevenson, A. Sakellariou, J. A. Taylor, Toolbox for advanced x-ray
434 image processing, in: *Proc Spie*, Vol. 8141, 2011, pp. 81410B–14.
- 435 [13] M. Born, E. Wolf, *Principles of optics: electromagnetic theory of propa-
436 gation, interference and diffraction of light*, Elsevier, 1980.
- 437 [14] M. Endrizzi, P. Oliva, B. Golosio, P. Delogu, Cmos aps detector character-
438 ization for quantitative x-ray imaging, *Nuclear Instruments and Methods
439 in Physics Research Section A: Accelerators, Spectrometers, Detectors
440 and Associated Equipment* 703 (2013) 26–32.

- 441 [15] D. Paganin, Coherent X-ray optics, no. 6, Oxford University Press on
442 Demand, 2006.
- 443 [16] R. James, The optical principles of the diffraction of x-rays, Bell and Sons,
444 1962.
- 445 [17] ICRU Tissue Substitutes in Radiation Dosimetry and Measurement, Re-
446 port 44 of the International Commission on Radiation Units and Measure-
447 ments, Bethesda, MD (1989).
- 448 [18] U. Bonse, M. Hart, An x-ray interferometer, Applied Physics Letters 6 (8)
449 (1965) 155–156.
- 450 [19] U. Bonse, M. Hart, An x-ray interferometer with long separated interfering
451 beam paths, Applied Physics Letters 7 (4) (1965) 99–100.
- 452 [20] M. Hart, U. Bonse, Interferometry with x rays, Physics Today 23 (8)
453 (1970) 26–31.
- 454 [21] J. H. Bruning, D. R. Herriott, J. Gallagher, D. Rosenfeld, A. White,
455 D. Brangaccio, Digital wavefront measuring interferometer for testing op-
456 tical surfaces and lenses, Applied optics 13 (11) (1974) 2693–2703.
- 457 [22] M. Ando, S. Hosoya, An attempt at x-ray phase-contrast microscopy,
458 in: Proceedings of the 6th International Conference on X-ray Optics and
459 Microanalysis. Tokyo: University of Tokyo Press, 1972, pp. 63–68.
- 460 [23] M. Hart, Review lecture: Ten years of x-ray interferometry, in: Proceed-
461 ings of the Royal Society of London A: Mathematical, Physical and Engi-
462 neering Sciences, Vol. 346, The Royal Society, 1975, pp. 1–22.
- 463 [24] A. Momose, Demonstration of phase-contrast x-ray computed tomogra-
464 phy using an x-ray interferometer, Nuclear Instruments and Methods in
465 Physics Research Section A: Accelerators, Spectrometers, Detectors and
466 Associated Equipment 352 (3) (1995) 622–628.

- 467 [25] T. Takeda, A. Momose, Y. Itai, W. Jin, K. Hirano, Phase-contrast imaging
468 with synchrotron x-rays for detecting cancer lesions, *Academic radiology*
469 2 (9) (1995) 799–803.
- 470 [26] A. Momose, T. Takeda, Y. Itai, Phase-contrast x-ray computed tomogra-
471 phy for observing biological specimens and organic materials, *Review of*
472 *scientific instruments* 66 (2) (1995) 1434–1436.
- 473 [27] A. Momose, T. Takeda, Y. Itai, K. Hirano, Phase-contrast x-ray com-
474 puted tomography for observing biological soft tissues, *Nature medicine*
475 2 (4) (1996) 473–475.
- 476 [28] T. Takeda, A. Momose, E. Ueno, Y. Itai, Phase-contrast x-ray ct image
477 of breast tumor, *Journal of synchrotron radiation* 5 (3) (1998) 1133–1135.
- 478 [29] A. Momose, J. Fukuda, Phase-contrast radiographs of nonstained rat cere-
479 bellar specimen, *Medical physics* 22 (4) (1995) 375–379.
- 480 [30] A. Momose, T. Takeda, Y. Itai, Contrast effect of blood on phase-contrast
481 x-ray imaging, *Academic radiology* 2 (10) (1995) 883–887.
- 482 [31] A. Snigirev, I. Snigireva, V. Kohn, S. Kuznetsov, I. Schelokov, On the pos-
483 sibilities of x-ray phase contrast microimaging by coherent high-energy
484 synchrotron radiation, *Review of scientific instruments* 66 (12) (1995)
485 5486–5492.
- 486 [32] P. Cloetens, R. Barrett, J. Baruchel, J.-P. Guigay, M. Schlenker, Phase
487 objects in synchrotron radiation hard x-ray imaging, *Journal of Physics*
488 *D: Applied Physics* 29 (1) (1996) 133.
- 489 [33] S. Wilkins, T. E. Gureyev, D. Gao, A. Pogany, A. Stevenson, Phase-
490 contrast imaging using polychromatic hard x-rays, *Nature* 384 (6607)
491 (1996) 335.
- 492 [34] K. A. Nugent, Coherent methods in the x-ray sciences, *Advances in*
493 *Physics* 59 (1) (2010) 1–99.

- 494 [35] A. Pogany, D. Gao, S. Wilkins, Contrast and resolution in imaging with
495 a microfocus x-ray source, *Review of Scientific Instruments* 68 (7) (1997)
496 2774–2782.
- 497 [36] Y. I. Nesterets, S. Wilkins, T. Gureyev, A. Pogany, A. Stevenson, On the
498 optimization of experimental parameters for x-ray in-line phase-contrast
499 imaging, *Review of scientific instruments* 76 (9) (2005) 093706.
- 500 [37] T. E. Gureyev, Y. I. Nesterets, A. W. Stevenson, P. R. Miller, A. Pogany,
501 S. W. Wilkins, Some simple rules for contrast, signal-to-noise and resolu-
502 tion in in-line x-ray phase-contrast imaging, *Optics express* 16 (5) (2008)
503 3223–3241.
- 504 [38] K. Nugent, T. Gureyev, D. Cookson, D. Paganin, Z. Barnea, Quantitative
505 phase imaging using hard x rays, *Physical review letters* 77 (14) (1996)
506 2961.
- 507 [39] T. Gureyev, S. Wilkins, On x-ray phase imaging with a point source,
508 *JOSA A* 15 (3) (1998) 579–585.
- 509 [40] T. Gureyev, C. Raven, A. Snigirev, I. Snigireva, S. Wilkins, Hard x-
510 ray quantitative non-interferometric phase-contrast microscopy, *Journal*
511 *of Physics D: Applied Physics* 32 (5) (1999) 563.
- 512 [41] T. E. Gureyev, C. Raven, A. A. Snigirev, I. Snigireva, S. W. Wilkins, Hard
513 x-ray quantitative noninterferometric phase-contrast imaging, in: *Medical*
514 *Imaging'99*, International Society for Optics and Photonics, 1999, pp. 356–
515 364.
- 516 [42] T. Gureyev, S. Wilkins, On x-ray phase retrieval from polychromatic im-
517 ages, *Optics communications* 147 (4) (1998) 229–232.
- 518 [43] T. Gureyev, S. Mayo, S. Wilkins, D. Paganin, A. Stevenson, Quantitative
519 in-line phase-contrast imaging with multienergy x rays, *Physical Review*
520 *Letters* 86 (25) (2001) 5827.

- 521 [44] P. Cloetens, W. Ludwig, J. Baruchel, D. Van Dyck, J. Van Landuyt,
522 J. Guigay, M. Schlenker, Holotomography: Quantitative phase tomogra-
523 phy with micrometer resolution using hard synchrotron radiation x rays,
524 Applied physics letters 75 (19) (1999) 2912–2914.
- 525 [45] A. V. Bronnikov, Reconstruction formulas in phase-contrast tomography,
526 Optics Communications 171 (4) (1999) 239–244.
- 527 [46] A. Barty, K. Nugent, A. Roberts, D. Paganin, Quantitative phase tomog-
528 raphy, Optics Communications 175 (4) (2000) 329–336.
- 529 [47] D. Paganin, S. Mayo, T. E. Gureyev, P. R. Miller, S. W. Wilkins, Simul-
530 taneous phase and amplitude extraction from a single defocused image of
531 a homogeneous object, Journal of microscopy 206 (1) (2002) 33–40.
- 532 [48] P. Cloetens, M. Pateyron-Salomé, J. Buffiere, G. Peix, J. Baruchel,
533 F. Peyrin, M. Schlenker, Observation of microstructure and damage in
534 materials by phase sensitive radiography and tomography, Journal of Ap-
535 plied Physics 81 (9) (1997) 5878–5886.
- 536 [49] J.-Y. Buffière, E. Maire, P. Cloetens, G. Lormand, R. Fougères, Charac-
537 terization of internal damage in a mmc p using x-ray synchrotron phase
538 contrast microtomography, Acta materialia 47 (5) (1999) 1613–1625.
- 539 [50] P. Spanne, C. Raven, I. Snigireva, A. Snigirev, In-line holography and
540 phase-contrast microtomography with high energy x-rays, Physics in
541 Medicine and Biology 44 (3) (1999) 741.
- 542 [51] P. Bleuet, P. Cloetens, P. Gergaud, D. Mariolle, N. Chevalier, R. Tucoulou,
543 J. Susini, A. Chabli, A hard x-ray nanoprobe for scanning and projection
544 nanotomography, Review of scientific instruments 80 (5) (2009) 056101.
- 545 [52] M. Langer, A. Pacureanu, H. Suhonen, Q. Grimal, P. Cloetens, F. Peyrin,
546 X-ray phase nanotomography resolves the 3d human bone ultrastructure,
547 PloS one 7 (8) (2012) e35691.

- 548 [53] H. Suhonen, F. Xu, L. Helfen, C. Ferrero, P. Vladimirov, P. Cloetens, X-
549 ray phase contrast and fluorescence nanotomography for material studies,
550 *International Journal of Materials Research* 103 (2) (2012) 179–183.
- 551 [54] P. Varga, A. Pacureanu, M. Langer, H. Suhonen, B. Hesse, Q. Grimal,
552 P. Cloetens, K. Raum, F. Peyrin, Investigation of the three-dimensional
553 orientation of mineralized collagen fibrils in human lamellar bone using
554 synchrotron x-ray phase nano-tomography, *Acta biomaterialia* 9 (9) (2013)
555 8118–8127.
- 556 [55] M. Kitchen, D. Paganin, R. Lewis, N. Yagi, K. Uesugi, S. Mudie, On the
557 origin of speckle in x-ray phase contrast images of lung tissue, *Physics in
558 medicine and biology* 49 (18) (2004) 4335.
- 559 [56] S. B. Hooper, M. J. Kitchen, M. J. Wallace, N. Yagi, K. Uesugi, M. J.
560 Morgan, C. Hall, K. K. Siu, I. M. Williams, M. Siew, et al., Imaging lung
561 aeration and lung liquid clearance at birth, *The FASEB Journal* 21 (12)
562 (2007) 3329–3337.
- 563 [57] M. Kitchen, R. Lewis, M. Morgan, M. Wallace, M. Siew, K. Siu, A. Habib,
564 A. Fouras, N. Yagi, K. Uesugi, et al., Dynamic measures of regional lung
565 air volume using phase contrast x-ray imaging, *Physics in medicine and
566 biology* 53 (21) (2008) 6065.
- 567 [58] M. Kitchen, R. Lewis, N. Yagi, K. Uesugi, D. Paganin, S. Hooper,
568 G. Adams, S. Jureczek, J. Singh, C. Christensen, et al., Phase contrast
569 x-ray imaging of mice and rabbit lungs: a comparative study, *The British
570 journal of radiology*.
- 571 [59] R. P. Murrie, K. S. Morgan, A. Maksimenko, A. Fouras, D. M. Paganin,
572 C. Hall, K. K. Siu, D. W. Parsons, M. Donnelley, Live small-animal x-
573 ray lung velocimetry and lung micro-tomography at the Australian syn-
574 chrotron imaging and medical beamline, *Journal of synchrotron radiation*
575 22 (4) (2015) 1049–1055.

- 576 [60] M. Di Michiel, A. Olivo, G. Tromba, F. Arfelli, V. Bonvicini, A. Bravin,
577 G. Cantatore, E. Castelli, L. D. Palma, R. Longo, S. Pani, D. Pontoni,
578 P. Poropat, M. Prest, A. Rashevsky, A. Vacchi, E. Vallazza, *Phase Con-*
579 *trast Imaging in the Field of Mammography*, Springer Japan, Tokyo, 1998,
580 pp. 78–82.
- 581 [61] F. Arfelli, M. Assante, V. Bonvicini, A. Bravin, G. Cantatore, E. Castelli,
582 L. D. Palma, M. D. Michiel, R. Longo, A. Olivo, S. Pani, D. Pontoni,
583 P. Poropat, M. Prest, A. Rashevsky, G. Tromba, A. Vacchi, E. Vallazza,
584 F. Zanconati, *Low-dose phase contrast x-ray medical imaging*, *Physics in*
585 *Medicine and Biology* 43 (10) (1998) 2845.
- 586 [62] E. Castelli, F. Arfelli, D. Dreossi, R. Longo, T. Rokvic, M. Cova, E. Quaia,
587 M. Tonutti, F. Zanconati, A. Abrami, et al., *Clinical mammography at*
588 *the syrmep beam line*, *Nuclear Instruments and Methods in Physics Re-*
589 *search Section A: Accelerators, Spectrometers, Detectors and Associated*
590 *Equipment* 572 (1) (2007) 237–240.
- 591 [63] E. Castelli, M. Tonutti, F. Arfelli, R. Longo, E. Quaia, L. Rigon, D. San-
592 abor, F. Zanconati, D. Dreossi, A. Abrami, et al., *Mammography with*
593 *synchrotron radiation: first clinical experience with phase-detection tech-*
594 *nique*, *Radiology* 259 (3) (2011) 684–694.
- 595 [64] R. Longo, M. Tonutti, L. Rigon, F. Arfelli, D. Dreossi, E. Quai, F. Zan-
596 conati, E. Castelli, G. Tromba, M. A. Cova, *Clinical study in phase-*
597 *contrast mammography: image-quality analysis*, *Philosophical Transac-*
598 *tions of the Royal Society of London A: Mathematical, Physical and En-*
599 *gineering Sciences* 372 (2010) (2014) 20130025.
- 600 [65] F. Arfelli, V. Bonvicini, A. Bravin, G. Cantatore, E. Castelli, L. D. Palma,
601 M. D. Michiel, M. Fabrizioli, R. Longo, R. H. Menk, et al., *Mammogra-*
602 *phy with synchrotron radiation: Phase-detection techniques 1*, *Radiology*
603 215 (1) (2000) 286–293.

- 604 [66] K. Goetz, M. Kalashnikov, Y. A. Mikhailov, G. V. Sklizkov, S. Fedotov,
605 E. Foerster, P. Zaumseil, Measurements of the parameters of shell targets
606 for laser thermonuclear fusion using an x-ray schlieren method, Soviet
607 Journal of Quantum Electronics 9 (5) (1979) 607.
- 608 [67] E. Forster, K. Goetz, P. Zaumseil, Double crystal diffractometry for the
609 characterization of targets for laser fusion experiments, Kristall und Tech-
610 nik 15 (8) (1980) 937–945.
- 611 [68] T. Davis, D. Gao, T. Gureyev, A. Stevenson, S. Wilkins, et al., Phase-
612 contrast imaging of weakly absorbing materials using hard x-rays, Nature
613 373 (6515) (1995) 595–598.
- 614 [69] V. Ingal, E. Beliaevskaya, X-ray plane-wave topography observation of
615 the phase contrast from a non-crystalline object, Journal of Physics D:
616 Applied Physics 28 (11) (1995) 2314.
- 617 [70] D. Chapman, W. Thomlinson, R. Johnston, D. Washburn, E. Pisano,
618 N. Gmür, Z. Zhong, R. Menk, F. Arfelli, D. Sayers, Diffraction enhanced
619 x-ray imaging, Physics in medicine and biology 42 (11) (1997) 2015.
- 620 [71] F. Dilmanian, Z. Zhong, B. Ren, X. Wu, L. Chapman, I. Orion, W. Thom-
621 linson, Computed tomography of x-ray index of refraction using the
622 diffraction enhanced imaging method, Physics in medicine and biology
623 45 (4) (2000) 933.
- 624 [72] Y. I. Nesterets, T. Gureyev, D. Paganin, K. Pavlov, S. Wilkins, Quan-
625 titative diffraction-enhanced x-ray imaging of weak objects, Journal of
626 Physics D: Applied Physics 37 (8) (2004) 1262.
- 627 [73] T. Gureyev, S. Wilkins, Regimes of x-ray phase-contrast imaging with
628 perfect crystals, Il Nuovo Cimento D 19 (2) (1997) 545–552.
- 629 [74] M. N. Wernick, O. Wirjadi, D. Chapman, Z. Zhong, N. P. Galatsanos,
630 Y. Yang, J. G. Brankov, O. Oltulu, M. A. Anastasio, C. Muehleman,

- 631 Multiple-image radiography, *Physics in medicine and biology* 48 (23)
632 (2003) 3875.
- 633 [75] O. Oltulu, Z. Zhong, M. Hasnah, M. N. Wernick, D. Chapman, Extraction
634 of extinction, refraction and absorption properties in diffraction enhanced
635 imaging, *Journal of Physics D: Applied Physics* 36 (17) (2003) 2152.
- 636 [76] L. Rigon, H.-J. Besch, F. Arfelli, R.-H. Menk, G. Heitner, H. Plothow-
637 Besch, A new dei algorithm capable of investigating sub-pixel structures,
638 *Journal of Physics D: Applied Physics* 36 (10A) (2003) A107.
- 639 [77] E. Pagot, P. Cloetens, S. Fiedler, A. Bravin, P. Coan, J. Baruchel,
640 J. Härtwig, W. Thomlinson, A method to extract quantitative information
641 in analyzer-based x-ray phase contrast imaging, *Applied Physics Letters*
642 82 (20) (2003) 3421–3423.
- 643 [78] L. Rigon, A. Astolfo, F. Arfelli, R.-H. Menk, Generalized diffraction en-
644 hanced imaging: application to tomography, *European journal of radiol-
645 ogy* 68 (3) (2008) S3–S7.
- 646 [79] M. J. Kitchen, D. M. Paganin, K. Uesugi, B. J. Allison, R. A. Lewis,
647 S. B. Hooper, K. M. Pavlov, X-ray phase, absorption and scatter retrieval
648 using two or more phase contrast images, *Optics express* 18 (19) (2010)
649 19994–20012.
- 650 [80] D. Chapman, E. Pisano, W. Thomlinson, Z. Zhong, R. Johnston, D. Wash-
651 burn, D. Sayers, K. Malinowska, Medical applications of diffraction en-
652 hanced imaging, *Breast Disease* 10 (3-4) (1998) 197–207.
- 653 [81] J. Mollenhauer, M. Aurich, Z. Zhong, C. Muehleman, A. Cole, M. Hasnah,
654 O. Oltulu, K. Kuettner, A. Margulis, L. Chapman, Diffraction-enhanced
655 x-ray imaging of articular cartilage, *Osteoarthritis and cartilage* 10 (3)
656 (2002) 163–171.
- 657 [82] P. Coan, F. Bamberg, P. C. Diemoz, A. Bravin, K. Timpert, E. Mützel,
658 J. G. Raya, S. Adam-Neumair, M. F. Reiser, C. Glaser, Characterization

- 659 of osteoarthritic and normal human patella cartilage by computed to-
660 mography x-ray phase-contrast imaging: a feasibility study, *Investigative*
661 *radiology* 45 (7) (2010) 437–444.
- 662 [83] P. Coan, A. Wagner, A. Bravin, P. C. Diemoz, J. Keyriläinen, J. Mollen-
663 hauer, In vivo x-ray phase contrast analyzer-based imaging for longitudi-
664 nal osteoarthritis studies in guinea pigs, *Physics in medicine and biology*
665 55 (24) (2010) 7649.
- 666 [84] C. Muehleman, J. Li, D. Connor, C. Parham, E. Pisano, Z. Zhong,
667 Diffraction-enhanced imaging of musculoskeletal tissues using a conven-
668 tional x-ray tube, *Academic radiology* 16 (8) (2009) 918–923.
- 669 [85] V. N. Ingal, E. A. Beliaevskaya, A. P. Brianskaya, R. D. Merkurieva,
670 Phase mammography—a new technique for breast investigation, *Physics in*
671 *medicine and biology* 43 (9) (1998) 2555.
- 672 [86] E. D. Pisano, R. E. Johnston, D. Chapman, J. Geradts, M. V. Iacocca,
673 C. A. Livasy, D. B. Washburn, D. E. Sayers, Z. Zhong, M. Z. Kiss, et al.,
674 Human breast cancer specimens: Diffraction-enhanced imaging with his-
675 tologic correlation?improved conspicuity of lesion detail compared with
676 digital radiography 1, *Radiology* 214 (3) (2000) 895–901.
- 677 [87] A. Sztrókay, P. Diemoz, T. Schlossbauer, E. Brun, F. Bamberg, D. Mayr,
678 M. Reiser, A. Bravin, P. Coan, High-resolution breast tomography at high
679 energy: a feasibility study of phase contrast imaging on a whole breast,
680 *Physics in medicine and biology* 57 (10) (2012) 2931.
- 681 [88] T. Millard, M. Endrizzi, L. Rigon, F. Arfelli, R. Menk, J. Owen, E. Stride,
682 A. Olivo, Quantification of microbubble concentration through x-ray
683 phase contrast imaging, *Applied Physics Letters* 103 (11) (2013) 114105.
- 684 [89] T. Millard, M. Endrizzi, N. Everdell, L. Rigon, F. Arfelli, R. Menk,
685 E. Stride, A. Olivo, Evaluation of microbubble contrast agents for dy-
686 namic imaging with x-ray phase contrast, *Scientific reports* 5.

- 687 [90] F. Pfeiffer, A. Momose, W. Yashiro, Milestones and basic principles of
688 grating-based x-ray and neutron phase-contrast imaging, in: AIP Confer-
689 ence Proceedings, Vol. 1466, AIP, 2012, pp. 2–11.
- 690 [91] J. Clauser, M. Reinsch, New theoretical and experimental results in fresnel
691 optics with applications to matter-wave and x-ray interferometry, Applied
692 Physics B: Lasers and Optics 54 (5) (1992) 380–395.
- 693 [92] J. F. Clauser, Ultrahigh resolution interferometric x-ray imaging, US
694 Patent 5,812,629.
- 695 [93] P. Cloetens, J. Guigay, C. De Martino, J. Baruchel, M. Schlenker, Frac-
696 tional talbot imaging of phase gratings with hard x rays, Optics letters
697 22 (14) (1997) 1059–1061.
- 698 [94] P. Cloetens, J.-P. Guigay, C. De Martino, M. Pateyron-Salome,
699 M. Schlenker, D. Van Dyck, Quantitative aspects of coherent hard x-
700 ray imaging: Talbot images and holographic reconstruction, in: Optical
701 Science, Engineering and Instrumentation'97, International Society for
702 Optics and Photonics, 1997, pp. 72–82.
- 703 [95] C. David, B. Nöhammer, H. Solak, E. Ziegler, Differential x-ray phase
704 contrast imaging using a shearing interferometer, Applied physics letters
705 81 (17) (2002) 3287–3289.
- 706 [96] A. Momose, S. Kawamoto, I. Koyama, Y. Hamaishi, K. Takai, Y. Suzuki,
707 Demonstration of x-ray talbot interferometry, Japanese journal of applied
708 physics 42 (7B) (2003) L866.
- 709 [97] T. Weitkamp, A. Diaz, C. David, F. Pfeiffer, M. Stampanoni, P. Cloetens,
710 E. Ziegler, X-ray phase imaging with a grating interferometer, Optics
711 express 13 (16) (2005) 6296–6304.
- 712 [98] F. Pfeiffer, T. Weitkamp, O. Bunk, C. David, Phase retrieval and dif-
713 ferential phase-contrast imaging with low-brilliance x-ray sources, Nature
714 physics 2 (4) (2006) 258–261.

- 715 [99] F. Pfeiffer, C. Kottler, O. Bunk, C. David, Hard x-ray phase tomography
716 with low-brilliance sources, *Physical review letters* 98 (10) (2007) 108105.
- 717 [100] F. Pfeiffer, M. Bech, O. Bunk, P. Kraft, E. F. Eikenberry, C. Brönnimann,
718 C. Grünzweig, C. David, Hard-x-ray dark-field imaging using a grating
719 interferometer, *Nature materials* 7 (2) (2008) 134–137.
- 720 [101] Z.-F. Huang, K.-J. Kang, L. Zhang, Z.-Q. Chen, F. Ding, Z.-T. Wang, Q.-
721 G. Fang, Alternative method for differential phase-contrast imaging with
722 weakly coherent hard x rays, *Physical Review A* 79 (1) (2009) 013815.
- 723 [102] Z.-T. Wang, K.-J. Kang, Z.-F. Huang, Z.-Q. Chen, Quantitative grating-
724 based x-ray dark-field computed tomography, *Applied Physics Letters*
725 95 (9) (2009) 094105.
- 726 [103] M. Bech, O. Bunk, T. Donath, R. Feidenhans, C. David, F. Pfeiffer, Quan-
727 titative x-ray dark-field computed tomography, *Physics in medicine and*
728 *biology* 55 (18) (2010) 5529.
- 729 [104] I. Zanette, T. Weitkamp, T. Donath, S. Rutishauser, C. David, Two-
730 dimensional x-ray grating interferometer, *Physical review letters* 105 (24)
731 (2010) 248102.
- 732 [105] H. Itoh, K. Nagai, G. Sato, K. Yamaguchi, T. Nakamura, T. Kondoh,
733 C. Ouchi, T. Teshima, Y. Setomoto, T. Den, Two-dimensional grating-
734 based x-ray phase-contrast imaging using fourier transform phase re-
735 trieval, *Optics express* 19 (4) (2011) 3339–3346.
- 736 [106] G. Sato, T. Kondoh, H. Itoh, S. Handa, K. Yamaguchi, T. Nakamura,
737 K. Nagai, C. Ouchi, T. Teshima, Y. Setomoto, et al., Two-dimensional
738 gratings-based phase-contrast imaging using a conventional x-ray tube,
739 *Optics letters* 36 (18) (2011) 3551–3553.
- 740 [107] B. Wu, Y. Liu, C. Rose-Petruck, G. J. Diebold, X-ray spatial frequency
741 heterodyne imaging, *Applied Physics Letters* 100 (6) (2012) 061110.

- 742 [108] T. Donath, M. Chabior, F. Pfeiffer, O. Bunk, E. Reznikova, J. Mohr,
743 E. Hempel, S. Popescu, M. Hoheisel, M. Schuster, et al., Inverse geom-
744 etry for grating-based x-ray phase-contrast imaging, *Journal of Applied*
745 *Physics* 106 (5) (2009) 054703.
- 746 [109] N. Morimoto, S. Fujino, K.-i. Ohshima, J. Harada, T. Hosoi, H. Watan-
747 abe, T. Shimura, X-ray phase contrast imaging by compact talbot-lau
748 interferometer with a single transmission grating, *Optics letters* 39 (15)
749 (2014) 4297–4300.
- 750 [110] H. Miao, A. A. Gomella, N. Chedid, L. Chen, H. Wen, Fabrication of 200
751 nm period hard x-ray phase gratings, *Nano letters* 14 (6) (2014) 3453.
- 752 [111] H. Miao, A. A. Gomella, K. J. Harmon, E. E. Bennett, N. Chedid, S. Znati,
753 A. Panna, B. A. Foster, P. Bhandarkar, H. Wen, Enhancing tabletop x-ray
754 phase contrast imaging with nano-fabrication, *Scientific reports* 5.
- 755 [112] H. Miao, A. Panna, A. A. Gomella, E. E. Bennett, S. Znati, L. Chen,
756 H. Wen, A universal moiré effect and application in x-ray phase-contrast
757 imaging, *Nature physics* 12 (9) (2016) 830–834.
- 758 [113] Z. Wang, N. Hauser, G. Singer, M. Trippel, R. A. Kubik-Huch, C. W.
759 Schneider, M. Stampanoni, Non-invasive classification of microcalcifica-
760 tions with phase-contrast x-ray mammography, *Nature communications*
761 5.
- 762 [114] T. Michel, J. Rieger, G. Anton, F. Bayer, M. W. Beckmann, J. Durst,
763 P. A. Fasching, W. Haas, A. Hartmann, G. Pelzer, et al., On a dark-
764 field signal generated by micrometer-sized calcifications in phase-contrast
765 mammography, *Physics in medicine and biology* 58 (8) (2013) 2713.
- 766 [115] M. Stampanoni, Z. Wang, T. Thüring, C. David, E. Roessl, M. Trippel,
767 R. A. Kubik-Huch, G. Singer, M. K. Hohl, N. Hauser, The first analysis
768 and clinical evaluation of native breast tissue using differential phase-
769 contrast mammography, *Investigative radiology* 46 (12) (2011) 801–806.

- 770 [116] F. Pfeiffer, O. Bunk, C. David, M. Bech, G. Le Duc, A. Bravin,
771 P. Cloetens, High-resolution brain tumor visualization using three-
772 dimensional x-ray phase contrast tomography, *Physics in medicine and*
773 *biology* 52 (23) (2007) 6923.
- 774 [117] A. Momose, W. Yashiro, K. Kido, J. Kiyohara, C. Makifuchi, T. Ito,
775 S. Nagatsuka, C. Honda, D. Noda, T. Hattori, et al., X-ray phase imaging:
776 from synchrotron to hospital, *Phil. Trans. R. Soc. A* 372 (2010) (2014)
777 20130023.
- 778 [118] J. Tanaka, M. Nagashima, K. Kido, Y. Hoshino, J. Kiyohara, C. Maki-
779 fuchi, S. Nishino, S. Nagatsuka, A. Momose, Cadaveric and in vivo human
780 joint imaging based on differential phase contrast by x-ray talbot-lau in-
781 terferometry, *Zeitschrift für medizinische Physik* 23 (3) (2013) 222–227.
- 782 [119] D. Stutman, T. J. Beck, J. A. Carrino, C. O. Bingham, Talbot phase-
783 contrast x-ray imaging for the small joints of the hand, *Physics in medicine*
784 *and biology* 56 (17) (2011) 5697.
- 785 [120] T. Thüring, R. Guggenberger, H. Alkadhi, J. Hodler, M. Vich, Z. Wang,
786 C. David, M. Stampanoni, Human hand radiography using x-ray differen-
787 tial phase contrast combined with dark-field imaging, *Skeletal radiology*
788 42 (6) (2013) 827–835.
- 789 [121] S. Schleede, F. G. Meinel, M. Bech, J. Herzen, K. Achterhold, G. Potdevin,
790 A. Malecki, S. Adam-Neumair, S. F. Thieme, F. Bamberg, et al., Emphy-
791 sema diagnosis using x-ray dark-field imaging at a laser-driven compact
792 synchrotron light source, *Proceedings of the National Academy of Sciences*
793 109 (44) (2012) 17880–17885.
- 794 [122] M. Bech, A. Tapfer, A. Velroyen, A. Yaroshenko, B. Pauwels, J. Hostens,
795 P. Bruyndonckx, A. Sasov, F. Pfeiffer, In-vivo dark-field and phase-
796 contrast x-ray imaging, *Scientific reports* 3 (2013) 3209.

- 797 [123] F. Pfeiffer, J. Herzen, M. Willner, M. Chabior, S. Auweter, M. Reiser,
798 F. Bamberg, Grating-based x-ray phase contrast for biomedical imaging
799 applications, *Zeitschrift für medizinische Physik* 23 (3) (2013) 176–185.
- 800 [124] S. Wilkins, Improved x-ray optics, especially for phase-contrast imaging,
801 International patent WO 1995005725 (1995) A1.
- 802 [125] S. Wilkins, On a spatially resolving usaxs instrument for operation at
803 a third-generation synchrotron radiation source, *Journal of synchrotron*
804 *radiation* 5 (3) (1998) 986–988.
- 805 [126] S. C. Mayo, B. Sexton, Refractive microlens array for wave-front analysis
806 in the medium to hard x-ray range, *Optics letters* 29 (8) (2004) 866–868.
- 807 [127] M. De Jonge, B. Hornberger, C. Holzner, D. Legnini, D. Paterson, I. Mc-
808 Nulty, C. Jacobsen, S. Vogt, Quantitative phase imaging with a scanning
809 transmission x-ray microscope, *Physical review letters* 100 (16) (2008)
810 163902.
- 811 [128] K. S. Morgan, D. M. Paganin, K. K. Siu, Quantitative single-exposure x-
812 ray phase contrast imaging using a single attenuation grid, *Optics express*
813 19 (20) (2011) 19781–19789.
- 814 [129] F. A. Vittoria, M. Endrizzi, P. C. Diemoz, U. H. Wagner, C. Rau,
815 I. K. Robinson, A. Olivo, Virtual edge illumination and one dimensional
816 beam tracking for absorption, refraction, and scattering retrieval, *Applied*
817 *Physics Letters* 104 (13) (2014) 134102.
- 818 [130] F. A. Vittoria, G. K. Kallon, D. Basta, P. C. Diemoz, I. K. Robinson,
819 A. Olivo, M. Endrizzi, Beam tracking approach for single-shot retrieval
820 of absorption, refraction, and dark-field signals with laboratory x-ray
821 sources, *Applied Physics Letters* 106 (22) (2015) 224102.
- 822 [131] K. S. Morgan, D. M. Paganin, K. K. Siu, Quantitative x-ray phase-
823 contrast imaging using a single grating of comparable pitch to sample
824 feature size, *Optics letters* 36 (1) (2011) 55–57.

- 825 [132] R. Cerbino, L. Peverini, M. Potenza, A. Robert, P. Bösecke, M. Giglio,
826 X-ray-scattering information obtained from near-field speckle, *Nature*
827 *Physics* 4 (3) (2008) 238–243.
- 828 [133] K. S. Morgan, D. M. Paganin, K. K. Siu, X-ray phase imaging with a
829 paper analyzer, *Applied Physics Letters* 100 (12) (2012) 124102.
- 830 [134] F. Krejci, J. Jakubek, M. Kroupa, Hard x-ray phase contrast imaging
831 using single absorption grating and hybrid semiconductor pixel detector,
832 *Review of Scientific Instruments* 81 (11) (2010) 113702.
- 833 [135] H. Wen, E. E. Bennett, M. M. Hegedus, S. C. Carroll, Spatial harmonic
834 imaging of x-ray scattering?initial results, *IEEE transactions on medical*
835 *imaging* 27 (8) (2008) 997–1002.
- 836 [136] H. H. Wen, E. E. Bennett, R. Kopace, A. F. Stein, V. Pai, Single-shot x-ray
837 differential phase-contrast and diffraction imaging using two-dimensional
838 transmission gratings, *Optics letters* 35 (12) (2010) 1932–1934.
- 839 [137] F. Krejci, J. Jakubek, M. Kroupa, Low dose x-ray phase contrast imaging
840 sensitive to phase effects in 2-d, in: *Nuclear Science Symposium Confer-*
841 *ence Record (NSS/MIC)*, 2010 IEEE, IEEE, 2010, pp. 2194–2199.
- 842 [138] S. Bérújon, E. Ziegler, R. Cerbino, L. Peverini, Two-dimensional x-ray
843 beam phase sensing, *Physical review letters* 108 (15) (2012) 158102.
- 844 [139] S. Berujon, H. Wang, K. Sawhney, X-ray multimodal imaging using a
845 random-phase object, *Physical Review A* 86 (6) (2012) 063813.
- 846 [140] I. Zanette, T. Zhou, A. Burvall, U. Lundström, D. H. Larsson, M. Zdora,
847 P. Thibault, F. Pfeiffer, H. M. Hertz, Speckle-based x-ray phase-contrast
848 and dark-field imaging with a laboratory source, *Physical review letters*
849 112 (25) (2014) 253903.
- 850 [141] T. H. Jensen, M. Bech, O. Bunk, T. Donath, C. David, R. Feidenhans,
851 F. Pfeiffer, Directional x-ray dark-field imaging, *Physics in medicine and*
852 *biology* 55 (12) (2010) 3317.

- 853 [142] H. Wang, S. Berujon, J. Herzen, R. Atwood, D. Laundry, A. Hipp, K. Sawh-
854 ney, X-ray phase contrast tomography by tracking near field speckle, Sci-
855 entific reports 5 (2015) 8762.
- 856 [143] M. Kagias, Z. Wang, P. Villanueva-Perez, K. Jefimovs, M. Stampanoni,
857 2d-omnidirectional hard-x-ray scattering sensitivity in a single shot, Phys-
858 ical review letters 116 (9) (2016) 093902.
- 859 [144] F. A. Vittoria, M. Endrizzi, P. C. Diemoz, A. Zamir, U. H. Wagner,
860 C. Rau, I. K. Robinson, A. Olivo, X-ray absorption, phase and dark-field
861 tomography through a beam tracking approach, Scientific reports 5 (2015)
862 16318.
- 863 [145] H. Wen, E. E. Bennett, M. M. Hegedus, S. Rapacchi, Fourier x-ray scat-
864 tering radiography yields bone structural information 1, Radiology 251 (3)
865 (2009) 910–918.
- 866 [146] K. S. Morgan, M. Donnelley, D. M. Paganin, A. Fouras, N. Yagi,
867 Y. Suzuki, A. Takeuchi, K. Uesugi, R. C. Boucher, D. W. Parsons, et al.,
868 Measuring airway surface liquid depth in ex vivo mouse airways by x-ray
869 imaging for the assessment of cystic fibrosis airway therapies, PloS one
870 8 (1) (2013) e55822.
- 871 [147] K. S. Morgan, M. Donnelley, N. Farrow, A. Fouras, N. Yagi, Y. Suzuki,
872 A. Takeuchi, K. Uesugi, R. C. Boucher, K. K. Siu, et al., In vivo x-
873 ray imaging reveals improved airway surface hydration after a therapy
874 designed for cystic fibrosis, American journal of respiratory and critical
875 care medicine 190 (4) (2014) 469–472.
- 876 [148] S. Berujon, H. Wang, S. Alcock, K. Sawhney, At-wavelength metrology of
877 hard x-ray mirror using near field speckle, Optics express 22 (6) (2014)
878 6438–6446.
- 879 [149] S. Berujon, E. Ziegler, P. Cloetens, X-ray pulse wavefront metrology using
880 speckle tracking, Journal of synchrotron radiation 22 (4) (2015) 886–894.

- 881 [150] A. Olivo, F. Arfelli, G. Cantatore, R. Longo, R. Menk, S. Pani, M. Prest,
882 P. Poropat, L. Rigon, G. Tromba, et al., An innovative digital imaging
883 set-up allowing a low-dose approach to phase contrast applications in the
884 medical field, *Medical physics* 28 (8) (2001) 1610–1619.
- 885 [151] P. R. Munro, K. Ignatyev, R. D. Speller, A. Olivo, Phase and absorp-
886 tion retrieval using incoherent x-ray sources, *Proceedings of the National*
887 *Academy of Sciences* 109 (35) (2012) 13922–13927.
- 888 [152] A. Olivo, R. Speller, A coded-aperture technique allowing x-ray phase
889 contrast imaging with conventional sources, *Applied Physics Letters* 91 (7)
890 (2007) 074106.
- 891 [153] P. R. Munro, K. Ignatyev, R. D. Speller, A. Olivo, Source size and tem-
892 poral coherence requirements of coded aperture type x-ray phase contrast
893 imaging systems., *Optics express* 18 (19) (2010) 19681–19692.
- 894 [154] M. Endrizzi, F. A. Vittoria, G. Kallon, D. Basta, P. C. Diemoz, A. Vin-
895 cenzi, P. Delogu, R. Bellazzini, A. Olivo, Achromatic approach to phase-
896 based multi-modal imaging with conventional x-ray sources, *Optics ex-*
897 *press* 23 (12) (2015) 16473–16480.
- 898 [155] P. Diemoz, M. Endrizzi, C. Zapata, Z. Pešić, C. Rau, A. Bravin, I. Robin-
899 son, A. Olivo, X-ray phase-contrast imaging with nanoradian angular res-
900 olution, *Physical review letters* 110 (13) (2013) 138105.
- 901 [156] P. Diemoz, C. Hagen, M. Endrizzi, A. Olivo, Sensitivity of laboratory
902 based implementations of edge illumination x-ray phase-contrast imaging,
903 *Applied Physics Letters* 103 (24) (2013) 244104.
- 904 [157] M. Endrizzi, F. Vittoria, L. Rigon, D. Dreossi, F. Iacoviello, P. Shear-
905 ing, A. Olivo, X-ray phase-contrast radiography and tomography with a
906 multiaperture analyzer, *Physical Review Letters* 118 (24) (2017) 243902.
- 907 [158] T. Millard, M. Endrizzi, K. Ignatyev, C. Hagen, P. Munro, R. Speller,
908 A. Olivo, Method for automatization of the alignment of a laboratory

- 909 based x-ray phase contrast edge illumination system, *Review of Scientific*
910 *Instruments* 84 (8) (2013) 083702.
- 911 [159] M. Endrizzi, D. Basta, A. Olivo, Laboratory-based x-ray phase-contrast
912 imaging with misaligned optical elements, *Applied Physics Letters*
913 107 (12) (2015) 124103.
- 914 [160] D. Basta, M. Endrizzi, F. Vittoria, G. Kallon, T. Millard, P. Diemoz,
915 A. Olivo, Note: Design and realization of a portable edge illumination x-
916 ray phase contrast imaging system, *Review of Scientific Instruments* 86 (9)
917 (2015) 096102.
- 918 [161] D. Basta, M. Endrizzi, F. Vittoria, A. Astolfo, A. Olivo, Compact and cost
919 effective lab-based edge-illumination x-ray phase contrast imaging with a
920 structured focal spot, *Applied Physics Letters* 108 (22) (2016) 224102.
- 921 [162] M. Endrizzi, F. A. Vittoria, P. C. Diemoz, R. Lorenzo, R. D. Speller, U. H.
922 Wagner, C. Rau, I. K. Robinson, A. Olivo, Phase-contrast microscopy at
923 high x-ray energy with a laboratory setup, *Optics letters* 39 (11) (2014)
924 3332–3335.
- 925 [163] G. K. Kallon, M. Wesolowski, F. A. Vittoria, M. Endrizzi, D. Basta, T. P.
926 Millard, P. C. Diemoz, A. Olivo, A laboratory based edge-illumination x-
927 ray phase-contrast imaging setup with two-directional sensitivity, *Applied*
928 *Physics Letters* 107 (20) (2015) 204105.
- 929 [164] M. Endrizzi, P. C. Diemoz, T. P. Millard, J. Louise Jones, R. D. Speller,
930 I. K. Robinson, A. Olivo, Hard x-ray dark-field imaging with incoherent
931 sample illumination, *Applied Physics Letters* 104 (2) (2014) 024106.
- 932 [165] M. Endrizzi, P. C. Diemoz, C. K. Hagen, T. P. Millard, F. A. Vitto-
933 ria, U. H. Wagner, C. Rau, I. K. Robinson, A. Olivo, Laboratory-based
934 edge-illumination phase-contrast imaging: Dark-field retrieval and high-
935 resolution implementations, in: *Nuclear Science Symposium and Medical*
936 *Imaging Conference (NSS/MIC)*, 2014 IEEE, IEEE, 2014, pp. 1–4.

- 937 [166] A. Astolfo, M. Endrizzi, G. Kallon, T. P. Millard, F. A. Vittoria, A. Olivo,
938 A first investigation of accuracy, precision and sensitivity of phase-based
939 x-ray dark-field imaging, *Journal of Physics D: Applied Physics* 49 (48)
940 (2016) 485501.
- 941 [167] C. Hagen, P. Diemoz, M. Endrizzi, L. Rigon, D. Dreossi, F. Arfelli,
942 F. Lopez, R. Longo, A. Olivo, Theory and preliminary experimental verifi-
943 cation of quantitative edge illumination x-ray phase contrast tomography,
944 *Optics express* 22 (7) (2014) 7989–8000.
- 945 [168] C. Hagen, P. Munro, M. Endrizzi, P. Diemoz, A. Olivo, Low-dose phase
946 contrast tomography with conventional x-ray sources, *Medical physics*
947 41 (7).
- 948 [169] C. K. Hagen, A. Zamir, P. C. Diemoz, M. Endrizzi, F. Kennedy, R. H.
949 Jager, A. Olivo, Low-dose x-ray phase contrast tomography: Experimental
950 setup, image reconstruction and applications in biomedicine, in: *Nuclear
951 Science Symposium and Medical Imaging Conference (NSS/MIC), 2014
952 IEEE, IEEE, 2014, pp. 1–5.*
- 953 [170] C. K. Hagen, M. Endrizzi, P. C. Diemoz, A. Olivo, Reverse projection
954 retrieval in edge illumination x-ray phase contrast computed tomography,
955 *Journal of Physics D: Applied Physics* 49 (25) (2016) 255501.
- 956 [171] C. K. Hagen, P. Maghsoudlou, G. Totonelli, P. C. Diemoz, M. Endrizzi,
957 A. Zamir, P. Coan, A. Bravin, P. De Coppi, A. Olivo, Strategies for fast
958 and low-dose laboratory-based phase contrast tomography for microstruc-
959 tural scaffold analysis in tissue engineering, in: *SPIE Optical Engineer-
960 ing+ Applications, International Society for Optics and Photonics, 2016,
961 pp. 996705–996705.*
- 962 [172] A. Zamir, M. Endrizzi, C. K. Hagen, F. A. Vittoria, L. Urbani,
963 P. De Coppi, A. Olivo, Robust phase retrieval for high resolution edge
964 illumination x-ray phase-contrast computed tomography in non-ideal en-
965 vironments, *Scientific Reports* 6.

- 966 [173] A. Zamir, C. K. Hagen, P. C. Diemoz, M. Endrizzi, F. A. Vittoria, L. Urbani, P. De Coppi, A. Olivo, Increased robustness and speed in low-dose phase-contrast tomography with laboratory sources, in: SPIE Optical Engineering+ Applications, International Society for Optics and Photonics, 2016, pp. 996716–996716.
- 967
968
969
970
- 971 [174] P. C. Diémoz, F. A. Vittoria, C. K. Hagen, M. Endrizzi, P. Coan, A. Bravin, U. H. Wagner, C. Rau, I. K. Robinson, A. Olivo, A single-image retrieval method for edge illumination x-ray phase-contrast imaging: application and noise analysis, *Physica Medica* 32 (12) (2016) 1759–1764.
- 972
973
974
- 975 [175] P. Diemoz, C. Hagen, M. Endrizzi, M. Minuti, R. Bellazzini, L. Urbani, P. De Coppi, A. Olivo, Single-shot x-ray phase-contrast computed tomography with nonmicrofocal laboratory sources, *Physical Review Applied* 7 (4) (2017) 044029.
- 976
977
978
- 979 [176] A. Zamir, P. C. Diemoz, F. A. Vittoria, C. K. Hagen, M. Endrizzi, A. Olivo, Edge illumination x-ray phase tomography of multi-material samples using a single-image phase retrieval algorithm, *Optics Express* 25 (10) (2017) 11984–11996.
- 980
981
982
- 983 [177] A. Olivo, S. Gkoumas, M. Endrizzi, C. Hagen, M. Szafraniec, P. Diemoz, P. Munro, K. Ignatyev, B. Johnson, J. Horrocks, et al., Low-dose phase contrast mammography with conventional x-ray sources, *Medical physics* 40 (9).
- 984
985
986
- 987 [178] P. C. Diemoz, A. Bravin, A. Sztrókay-Gaul, M. Ruat, S. Grandl, D. Mayr, S. Auweter, A. Mittone, E. Brun, C. Ponchut, et al., A method for high-energy, low-dose mammography using edge illumination x-ray phase-contrast imaging, *Physics in Medicine and Biology* 61 (24) (2016) 8750.
- 988
989
990
- 991 [179] M. Marenzana, C. K. Hagen, P. D. N. Borges, M. Endrizzi, M. B. Szafraniec, K. Ignatyev, A. Olivo, Visualization of small lesions in rat cartilage by means of laboratory-based x-ray phase contrast imaging, *Physics in medicine and biology* 57 (24) (2012) 8173.
- 992
993
994

- 995 [180] M. Marenzana, C. K. Hagen, P. D. N. Borges, M. Endrizzi, M. B.
996 Szafraniec, T. L. Vincent, L. Rigon, F. Arfelli, R.-H. Menk, A. Olivo,
997 Synchrotron-and laboratory-based x-ray phase-contrast imaging for imag-
998 ing mouse articular cartilage in the absence of radiopaque contrast agents,
999 Philosophical Transactions of the Royal Society of London A: Mathemat-
1000 ical, Physical and Engineering Sciences 372 (2010) (2014) 20130127.
- 1001 [181] K. Ignatyev, P. Munro, D. Chana, R. Speller, A. Olivo, Coded apertures
1002 allow high-energy x-ray phase contrast imaging with laboratory sources,
1003 Journal of Applied Physics 110 (1) (2011) 014906.
- 1004 [182] A. Astolfo, M. Endrizzi, B. Price, I. Haig, A. Olivo, The first large-
1005 area, high-x-ray energy phase contrast prototype for enhanced detection
1006 of threat objects in baggage screening, in: SPIE Security+ Defence, In-
1007 ternational Society for Optics and Photonics, 2016, pp. 999504–999504.
- 1008 [183] M. Endrizzi, A. Astolfo, F. A. Vittoria, T. P. Millard, A. Olivo, Asym-
1009 metric masks for laboratory-based x-ray phase-contrast imaging with edge
1010 illumination, Scientific reports 6.
- 1011 [184] M. Endrizzi, A. Astolfo, B. Price, I. Haig, A. Olivo, Asymmetric masks for
1012 large field-of-view and high-energy x-ray phase contrast imaging, Journal
1013 of Instrumentation 11 (12) (2016) C12009.
- 1014 [185] A. Astolfo, M. Endrizzi, F. A. Vittoria, P. C. Diemoz, B. Price, I. Haig,
1015 A. Olivo, Large field of view, fast and low dose multimodal phase-contrast
1016 imaging at high x-ray energy, Scientific Reports 7.
- 1017 [186] M. Endrizzi, B. Murat, P. Fromme, A. Olivo, Edge-illumination x-ray
1018 dark-field imaging for visualising defects in composite structures, Com-
1019 posite Structures 134 (2015) 895–899.
- 1020 [187] M. Endrizzi, A. Astolfo, B. Price, I. Haig, A. Olivo, Large field-of-view
1021 asymmetric masks for high-energy x-ray phase imaging with standard x-

- 1022 ray tube, in: SPIE Optical Engineering+ Applications, International So-
1023 ciety for Optics and Photonics, 2016, pp. 99640A–99640A.
- 1024 [188] C. K. Hagen, P. Maghsoudlou, G. Totonelli, P. C. Diemoz, M. Endrizzi,
1025 L. Rigon, R.-H. Menk, F. Arfelli, D. Dreossi, E. Brun, et al., High contrast
1026 microstructural visualization of natural acellular matrices by means of
1027 phase-based x-ray tomography, *Scientific reports* 5 (2015) 18156.
- 1028 [189] P. Modregger, T. P. Cremona, C. Benarafa, J. C. Schittny, A. Olivo,
1029 M. Endrizzi, Small angle x-ray scattering with edge-illumination, *Scientific*
1030 *Reports* 6.